J. exp. Biol. **148**, 19–52 (1990)
Printed in Great Britain © *The Company of Biologists Limited 1990*

MECHANICS OF FORWARD FLIGHT IN BUMBLEBEES

I. KINEMATICS AND MORPHOLOGY

BY R. DUDLEY* AND C. P. ELLINGTON

Department of Zoology, University of Cambridge, Downing Street, Cambridge CB2 3EJ, United Kingdom

Accepted 2 June 1989

Summary

Using high-speed cinematography, bumblebees in free flight were filmed over a range of forward airspeeds. A detailed description of the wing tip and body kinematics was obtained from a three-dimensional reconstruction of the two-dimensional film image. A technique for determining quantitatively the angle of attack of the wing was developed. Kinematic parameters found to vary consistently with airspeed were body angle, stroke plane angle, geometrical angle of attack, and rotational angles of the wings at the ends of half-strokes. Results of a morphological analysis of the wings and bodies of those insects filmed in free flight are presented for use in later calculations of the lift and power requirements of forward flight.

Introduction

An accurate description of the wing and body kinematics of flying insects is fundamental to any analysis of the associated mechanics and aerodynamics of forward flight. Traditionally, studies of insect flight kinematics have been performed on tethered insects (Hollick, 1940; Jensen, 1956; Weis-Fogh, 1956; Nachtigall, 1966; Vogel, 1966, 1967; Zarnack, 1972). Kinematic parameters investigated in these studies have included wingbeat frequency, motion of the wing tip and wing profile. Weis-Fogh (1973) initiated a new era in animal flight research with his study of free hovering flight in insects, and this method of analysis has since become increasingly sophisticated (Ellington, 1980, 1984*b*). Detailed analyses of wingbeat kinematics and wake geometries of free-flying bats and birds have also become increasingly popular (e.g. Norberg, 1976; Rayner *et al.* 1986; Spedding, 1986, 1987). Particular attention has been paid in these studies to the variation of kinematic parameters with forward airspeed, in order to determine the means by which aerodynamic force is produced and its direction and magnitude regulated.

Comparable analysis of the forward flight of insects has not been possible until recently. The absence of detailed kinematic studies of free forward flight in insects

* Present address: Smithsonian Tropical Research Institute, APO Miami, FL 34002, USA.

Key words: flight, kinematics, bumblebees.

can be attributed to the technical difficulties of eliciting controlled, properly oriented flight for significant periods of time. The alternative method, tethering, introduces a variety of behavioral and mechanical constraints (Ellington, 1984*b*); it is unknown how similar the wing kinematics observed in tethered insects are to those in free flight. Only for one insect species, the migratory locust, are there kinematic data available for a direct comparison of free and tethered flight. Baker *et al.* (1981) showed that the wingbeat frequency of locusts in free flight was typically 16 % greater than that of tethered insects flying at some preferred speed and that, on average, speeds in free flight were some 39 % greater than preferred speeds in tethered flight. It was also shown by Kutsch & Stevenson (1981) that the wingbeat frequency of tethered locusts was significantly less than that of individuals in free flight, for both juvenile and mature individuals.

It is clear that kinematic studies of insects in free flight avoid all the potential limitations imposed by tethering. The best method for controlling free flight in insects is probably to rely upon their optomotor responses; through a judicious, perhaps fortuitous, choice of lighting and moving optical cues, it should be possible to elicit controlled flight (e.g. David, 1979). The present paper describes the experimental methodology and means of analysis used to determine the wing and body kinematics of bumblebees in free forward flight. An optomotor system consisting of moving stripes and fixed lighting is described whereby the orientation and general quality of flight in insects can be controlled. High-speed ciné films were taken of bumblebees flying over a range of forward airspeeds. A projection analysis was used to reconstruct the three-dimensional position of the wing tip and the body from single-view ciné frames. The variation of kinematic parameters with forward airspeed was examined in detail. A detailed morphological analysis was also carried out for those bumblebees filmed in free flight to provide data for calculations of lift and power requirements (Dudley & Ellington, 1990).

A new method is presented for the analysis of the span-wise angle of attack of the wings. This method, based upon the bilateral symmetry of wing motions, allows determination from a single view of the three-dimensional position of arbitrarily chosen points along the wing margin. A detailed description of the orientation of the wing through the wingbeat and at different airspeeds is thereby obtained. Such an approach is computationally and logistically simpler than more traditional methods of stereophotogrammetry, and is more generally applicable to three-dimensional reconstruction from a single view of the position and orientation of symmetrically paired animal appendages. This technique is used to measure for flying bumblebees the angle of attack of the wing through the wingbeat, and to examine in detail the variation of wing orientation with forward airspeed.

Materials and methods

Insects

Bumblebees, because of their size, general availability in the summer months,

and noted ability to hover and to sustain forward flight, were chosen as the model insect for the present study. All experimental work in the present paper was performed on the buff-tailed bumblebee *Bombus terrestris* (L.) *sensu* Alford (1975), and all future text references to bumblebees refer to this species. Insects were collected in the Cambridge University Botanic Garden and were usually filmed within a day. They were maintained in large well-ventilated cages and were fed a dilute mixture of honey and water (50% v/v). Only the most vigorous individuals were selected for filming.

Filming

The wind tunnel used in all experiments was the same open-jet tunnel as used by Weis-Fogh & Jensen (1956), wherein a detailed description of the tunnel design may be found. The original motor was replaced with a variable-speed d.c. motor for better speed control. A bead thermistor anemometer (Prosser AVM 502) was used to determine velocity profiles in the region of the working section where insects were filmed. Mean air velocities at each of six different points, all located in the general region of the working section where flight was filmed, were found typically to be within 1% of the designated free-stream value, over a range of 1–5 $m\,s^{-1}$. At any one point, measured velocity fluctuations were typically within 3% of the mean value, with a dominant frequency in the range 6–10 Hz at an airspeed of 3 $m\,s^{-1}$.

The working section of the open-jet tunnel was enclosed by a cylindrical section of 2 mm acetate sheet (Fig. 1A); the enclosed working section was 280 mm in length and 140 mm in diameter. Insects were kept within the working section by a circular piece of coarse-weave fabric at the downstream end, and by a fine plastic netting fitted between the front of the working section and the opening of the wind tunnel upstream. A 60° sector of the acetate sheet was removed and replaced with a 75 mm × 75 mm window of plate glass to reduce optical distortion in filming. Air velocity measurements with and without the window in place suggested that its effect on the airflow in the general region of flight was negligible.

Controlling the free flight of the insects proved to be difficult. A variety of

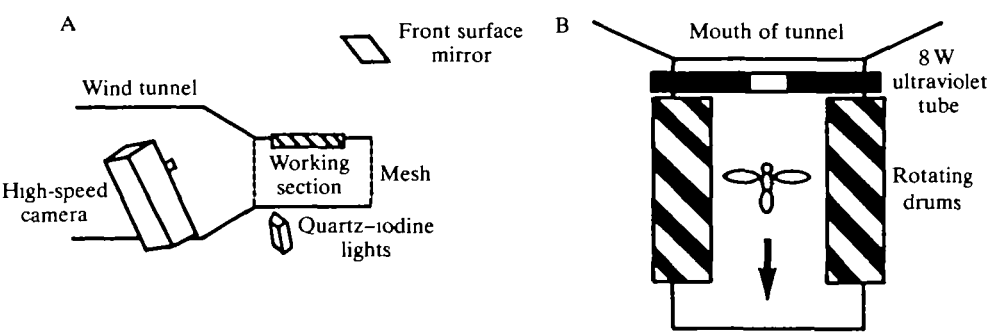

Fig. 1. (A) Lateral view of the working section and camera arrangement. (B) Vertical view of the working section. The arrow indicates the direction of air flow.

schemes was experimented with, and the most successful method to date is presented here: ultraviolet light proved to be a strong stimulus for initiating and sustaining flight, and a moving stripe pattern provided directional orientation. An 8 W Atlas ultraviolet fluorescent light was positioned above and perpendicular to the working section; most of the light was masked out such that only a small central section (approximately 3 cm in length) was visible (Fig. 1B). Above and on either side of the working section were positioned two rotating 'barber pole' drums 60 mm in diameter and 160 mm long. The exterior of each drum was covered with alternating black and white stripes at a pitch of 45°. The drum axles were linked mechanically such that the direction of stripe motion was the same for each drum. The drums were driven at 1–3 revs s^{-1} by a small d.c. motor; the speed of rotation was controlled remotely by the observer. Room temperature at the time of filming was always within 3° of 25°C.

A Hyspeed 16 mm ciné camera [John Hadland (P.I.), UK], fitted with a 75 mm Bolex lens at f/8, was used for all high-speed photography. The camera was operated at 5000 frames s^{-1}, which, for a typical bumblebee wingbeat frequency of 150 Hz, resulted in approximately 33 film frames per wingbeat. The camera arrangement can be seen in Fig. 1A. The insect image was reflected to the camera by a front surface mirror, which was positioned above and to the right of the working section. By virtue of the mirror tilt, the angle between the object plane and horizontal was 70°, while the angle between the longitudinal axis of the tunnel and the optical axis of the camera, when projected onto a horizontal plane, was 25°.

Backlighting of the insect provided a silhouette image for filming: sufficient contrast could not be obtained with front lighting, even when using 5 kW of illumination. Two 1 kW quartz–iodine lights were placed approximately 5 cm behind and underneath the far side of the working section (Fig. 1A). A sheet of translucent drafting film taped around the bottom of the working section acted as a light diffuser, giving a uniformly lit background against which the silhouette image of the flying insect could be seen.

The high-speed camera required approximately 0·5 s to reach a running speed of 5000 frames s^{-1}. To prevent film wastage, therefore, a 15·3 m film leader was spliced to the length of film to be exposed, the latter usually being 3·7 m in length and representing approximately 0·1 s of actual filming. A relay box turned on the camera lights approximately 0·5 s after the camera was triggered, at the same time that the beginning of the film to be exposed passed through the shutter mechanism. Any potentially adverse effects of the intense lighting on flight behavior were thus avoided in the 0·5 s prior to actual film exposure.

With the wind tunnel already up to speed, an insect was introduced into the working section. The drums were set rotating, and the ultraviolet light was then flickered on and off until the insect began to fly, at which point the light was left on. Several seconds of non-oriented and unsteady flight occurred before the insect 'locked on' to the moving stripes and began to fly steadily in the filming area of the working section. Flight duration ranged from less than 1 s to 1·5 min; a detailed

account of flight performance is given below in the Results section. After steady flight had been attained and the insect was positioned properly for filming, the high-speed camera was triggered. Immediately after the film had finished (approximately 0·75 s), the camera lights, ultraviolet light and rotating drums were all turned off. While the insect walked about inside the working section, a new film was put into the camera, and then the entire process was repeated. For a particular insect flying at one wind velocity, three filming attempts were usually necessary to guarantee at least one successful film in which the insect was properly oriented and the focus sufficient for analysis. Failure to obtain a good film was typically due to the unpredictable departure of the insect from the filming area in the 0·5 s before the camera reached full running speed.

Insects were filmed flying at three wind velocities (1, 2·5, and 4·5 $m\,s^{-1}$), and while hovering with the wind tunnel turned off. A video camera was also used to record all filming sessions, to identify those films in which the insect was in the field of view during filming, and also to ensure for films of hovering flight that in the seconds prior to actual filming the insect was in normal unaccelerated flight. The flight speeds used in this study correspond approximately to those typically found in nature. For example, Heinrich (1979) states that bumblebees fly to and from foraging sites at 3–5 $m\,s^{-1}$, while J. H. Mayberry (personal communication) has found that bumblebees foraging between artificial flowers spaced less than 1 m apart fly at speeds of less than 2 $m\,s^{-1}$.

Towards the end of filming sessions, insects displayed an increasing reluctance to fly at the higher velocities, but were almost always capable of hovering beneath the ultraviolet light. Filming was thus begun with flight at 4·5 $m\,s^{-1}$, and continued with successively lower velocities, culminating in the filming of hovering flight. An entire film sequence of flights over the indicated range of velocities could be obtained in less than 1 h, given a cooperative animal. Insects were weighed both before and after a filming sequence. Weight loss over the filming period was typically less than 10 % of the initial value, and therefore the mean of the two measurements was taken to be representative of the body mass during filmed flight.

Films were developed at 25 °C in a 1:9 solution of Ilford PQ developer and were fixed in a 1:3 solution of FX-Universal fixer. All films were analyzed using the projection equipment described by Ellington (1984*b*). A 12 bit A–D converter (CUBAN-12, Control Universal Ltd) was used to interface the digitizer to a Model B BBC microcomputer with a 6502 second processor. Computer programs for the kinematic analysis were written in HI-BASIC, an extended version of BBC BASIC.

Wing tip kinematics and body angle

The analysis of wing tip kinematics was generally the same as that used by Ellington (1984*b*), to which the reader is referred for further details. To analyze the motion of the wing tip through the course of a wingbeat, it was necessary to digitize for each film frame three points on the film image: the near wing base P_1

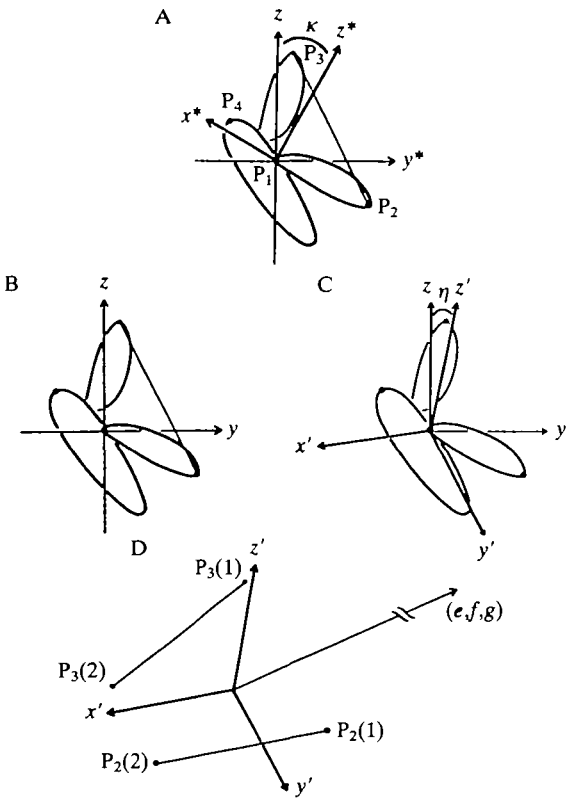

Fig. 2. Mutually orthogonal coordinate systems used in the kinematic analysis, modified from Ellington (1984*b*). (A) The filming coordinate system (x^*,y^*,z^*), with points P_1–P_4 used in the kinematic analysis. κ, camera tilt. (B) The (x,y,z) coordinate system. (C) The (x',y',z') coordinate system fixed in the insect body. (D) Method for determining a line parallel to the plane of symmetry. The line (e,f,g) is parallel to the plane.

(which was always the base of the left wing of the insect), the corresponding wing tip P_2, and the opposite or far wing tip P_3 (Fig. 2). Additional points of interest which will be considered later include the anterior tip of the body P_4, the far wing base P_5, and the point of intersection of the wing base axis with the median longitudinal plane of the body, P_6.

The image reconstruction technique relates the filming coordinate system to a coordinate system fixed in the insect body. Wing motions are presumed to be bilaterally symmetrical, and longitudinal bending of the wing is assumed to be insignificant. Initially, coordinates of the points of interest are given in the camera-based filming system (x^*,y^*,z^*), in which the y^* axis is horizontal and the x^* axis points along the optical axis of the camera (Fig. 2A). Coordinates are then transformed to the (x,y,z) system by rotating the filming coordinate system about the y^* axis (coincident with the y axis) until the x^* axis becomes the horizontal x

axis, with the z axis vertical (Fig. 2B). The (x,y,z) system is the same as Ellington's, who used a horizontal optical axis. Given a camera tilt above the horizontal of κ, coordinates in the (x^*,y^*,z^*) system can be expressed in the (x,y,z) system as follows:

$$x = x^*\cos(\kappa) - z^*\sin(\kappa)\,, \tag{1}$$

$$y = y^*\,, \tag{2}$$

$$z = x^*\sin(\kappa) + z^*\cos(\kappa)\,. \tag{3}$$

At this point, the analysis of wing tip kinematics then follows the previously published analysis: coordinates in the (x,y,z) system are transformed to the (x',y',z') system fixed in the insect body, such that the x' axis remains horizontal and parallel to the plane of symmetry, the y' axis is parallel to a line joining the wing tips, and the z' axis is not necessarily vertical (Fig. 2C). The coordinates of any point in the (x,y,z) system can be converted to (x',y',z') coordinates by means of a matrix of direction cosines (see below).

By virtue of the symmetry condition, there exists for any point P_7 on the near wing margin a corresponding point P_8 on the opposite wing margin (Fig. 3). This can be expressed in the (x',y',z') coordinate system by means of the following identities:

$$x'_7 = x'_8\,, \tag{4}$$

$$y'_7 = -y'_8 - B\,, \tag{5}$$

$$z'_7 = z'_8\,, \tag{6}$$

where B is the wing base separation. Similarly, for the near wing tip P_2 and the far wing tip P_3:

$$x'_2 = x'_3\,, \tag{7}$$

$$y'_2 = -y'_3 - B\,, \tag{8}$$

$$z'_2 = z'_3\,. \tag{9}$$

The untransformed coordinates of the far wing base P_5 are, of course, $(0,-B,0)$.

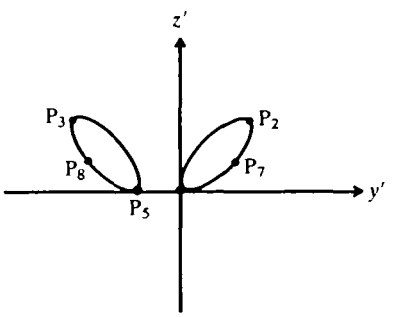

Fig. 3. In the (x',y',z') coordinate system, an arbitrary point P_7 on the near wing and its corresponding point P_8 on the opposite wing. P_2 is the near wing tip and P_3 the far wing tip; P_5 is the opposite wing base.

The origin of the filming coordinate system was always taken to be the near wing base P_1. The maximum projected wing length for the wingbeat sequence was determined and used to normalize all coordinates. To transform the digitized coordinates of the near and far wing tips to the (x,y,z) system, it is first necessary to calculate values of x^*. Since the near wing base is defined as the origin of the (x^*,y^*,z^*) system, the x^* coordinate of the near wing tip for each frame can be easily determined from the projected wing length. A more involved approach is, however, necessary to calculate the x_3^* coordinate of the far wing tip. In the (x^*,y^*,z^*) system, the direction of the line connecting the two wing tips can be given as $(a^*,1,c^*)$, which is entirely analogous to the direction $(a,1,c)$ in the (x,y,z) system, as given by Ellington (1984*b*), and is parallel to the y' axis for any viewing coordinate system. The direction number c^* is the slope on the film image of the line connecting the near and far wing tips; a mean slope $\bar{c}^*$, the value of c^* in each frame being weighted by the square of the projected line length, was calculated for a particular wingbeat sequence. The direction number a^* was calculated using positions $P(1)$ and $P(2)$ of both wing tips at either ends of the half-stroke (Fig. 2D; see Ellington, 1984*b*). A mean value of a^* was determined from several combinations of frames at either end of the wingbeat. Given knowledge of $\bar{a}^*$ and $\bar{c}^*$, values of x_3^* for the opposite wing tip can be calculated for each frame of the sequence. Coordinates of the near and far wing tips were then transformed to the (x,y,z) system using equations 1–3.

At this stage, the direction in the (x,y,z) system of the y' axis was determined; mean values of a and c, weighted by the square of the appropriate line length in each frame, were calculated for the (x,y,z) coordinate system. From these direction numbers, the direction cosines relating the (x,y,z) coordinate system to the (x',y',z') coordinate system fixed in the insect body could be determined. The near wing tip and far wing tip in the (x,y,z) system were then transformed, using the direction cosines, to the (x',y',z') system. A mean wing base separation for the sequence was calculated from the y' values of the near and far wing tips using equation 8.

The stroke plane angle β (Fig. 4) was determined from the slope of a linear regression of the x' and z' coordinates of the near wing tip. The wing tip position is

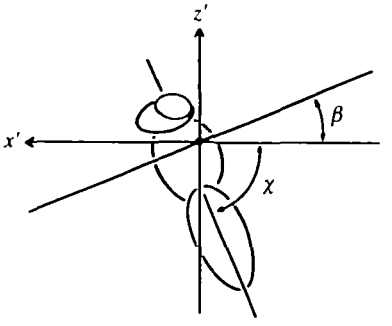

Fig. 4. Definition of the body angle χ and the stroke plane angle β.

defined by spherical coordinates, the positional angle ϕ and the angle of elevation θ, which are derived from a coordinate system based upon the stroke plane. Roll η of the insect is given by the angle between the z and z' axes, while yaw (deviation from the longitudinal axis of the tunnel) is given by the difference between the horizontal projection of the angle between the tunnel axis and the optical axis of the camera, 25°, and the angle between the x and x' axes. When the left wing is below horizontal, roll is negative; negative yaw corresponds to a yaw towards the right of the insect. Wingbeat frequency was determined from 1 ms timing marks on the film, account being taken of the film acceleration during a sequence.

Because of the orientation of the camera relative to the insect, it was not possible to determine accurately body angle χ (Fig. 4), or the three-dimensional position of the near wing base from the film image. Small errors in the measurements of points on the body could produce large errors in projected x^* coordinates of these points. Several attempts were made to photograph from the side of the working section insects that were simultaneously being filmed with the high-speed camera. Because of the problems of camera synchronization these efforts were abandoned, and an analytical technique was developed which relied upon both wing bases being visible on the film image. The y^* and z^* coordinates of the anterior tip of the body P_4 and the far wing base P_5 were digitized from the film image. From the mean wing base separation and the maximum projected length of the wing, the distance B between the wing bases was determined, and the x^* coordinate of the far wing base was calculated from:

$$x_5^* = -[B^2 - (y_5^*)^2 - (z_5^*)^2]^{1/2}. \tag{10}$$

The coordinates of the point of intersection P_6 of the wing base axis with the median longitudinal plane of the body are given by:

$$x_6^* = x_5^*/2, \tag{11}$$

$$y_6^* = y_5^*/2, \tag{12}$$

$$z_6^* = z_5^*/2. \tag{13}$$

The distance o from the point P_6 to the anterior tip of the body P_4 can be calculated from the morphological parameters given below. Namely, as a fraction of the body length:

$$\hat{o} = [\hat{l}^2 + \hat{l}_1^2 - 2\hat{l}\hat{l}_1\cos(90 - \chi_0)]^{1/2}, \tag{14}$$

when χ_0, the free body angle, is given in degrees. $\hat{l}$ and $\hat{l}_1$ are the distances of the center of mass from the anterior tip of the body and the wing base axis, respectively, divided by body length. The value of o is determined from $\hat{o}$ by scaling appropriately by the actual wing and body lengths and the maximum projected wing length of the sequence. Knowledge of the distance o permits a calculation of the x^* coordinate of P_4:

$$x_4^* = \pm[o^2 - (y_4^* - y_6^*)^2 - (z_4^* - z_6^*)^2]^{1/2}, \tag{15}$$

with the sign determined by the observer. Points P_4 and P_6 were then transformed

successively to the (x,y,z) system and to the (x',y',z') system. The body angle χ is then given by:

$$\chi = \tan^{-1}[(z'_4 - z'_6)/(x'_4 - x'_6)] + \lambda\,, \tag{16}$$

where

$$\lambda = \cos^{-1}[(\hat{l}^2 + \hat{o}^2 - \hat{l}_1^{\,2})/(2\hat{l}\hat{o})]\,.$$

Neglect of perspective effects in the reconstruction of the wing position from the film image introduces errors in the calculated spatial angles of the wing tip, and additionally results in a tilt of the assumed horizontal plane from the true horizontal (Ellington, 1984*b*). To determine the magnitude of these effects, it is necessary to know the horizontal coverage W of the film image and the distance Y from the object plane to the optical center of the lens. The quantities W and Y were about 5 and 80 wing lengths, respectively, for a typical insect in the filming arrangements described above. Given these values, the maximum error in the reconstructed spatial angles of the wing is calculated to be approximately 0·5°, and the angular tilt between the horizontal plane, based on the image projection and true horizontal, less than 1°.

Span-wise angle of attack

For a particular frame of a wingbeat sequence previously analyzed for wing tip kinematics, the three-dimensional configuration of the wing margins was determined as follows. Initially, the wing margins were digitized from the film image and stored in the computer. The x^* coordinates of all points on the margins were then calculated, and all coordinates in the filming coordinate system were transformed first to the (x,y,z) coordinate system and then to the insect coordinate system (x',y',z'). Finally, two rotations of the wing such that the longitudinal axis of the wing was coincident with the x' axis permitted the determination of the endpoints of a series of chords equally spaced along the wing span. When the wing was rotated back to its original position, these chords were then used to calculate the chord angle relative to horizontal at span-wise locations.

The span-wise angle of attack of wing chords was determined as follows. The near wing base P_1 was first digitized, and served as the origin for all points subsequently entered. The near and far wing tips P_2 and P_3 were then digitized, as was the far wing base P_5, if it was visible. Points were then entered along the wing margins, from wing tip to wing base, for each of four cases: near leading edge, near trailing edge, far leading edge, and far trailing edge. The maximum projected length R', as determined for the sequence by the previous wing tip analysis, was used to normalize all coordinates. The x^* coordinate of the near wing tip P_2 was also determined from the maximum projected wing length.

From the film image, the y^* and z^* coordinates of any point P_7 on the near wing margin are known. The y^* and z^* coordinates of the corresponding point P_8 on the opposite margin are, in general, unknown. It is readily apparent, however, that the line connecting these two points must be parallel to the line connecting the wing tips P_2 and P_3, given the assumption of bilateral symmetry of wing motions (see Fig. 3). In any two-dimensional projection the slope s of the line connecting

P_7 and P_8 is therefore equal to the slope of the line connecting the wing tips. In the (x^*,y^*,z^*) system of the film image, the y^* and z^* coordinates of the point P_8 can be found from the intersection with the far wing of a line with slope s passing through point P_7.

For each point P_7 on the near leading or near trailing edge, therefore, the equation of a line with slope s passing through that point was determined. The point of intersection of this line with the far leading or far trailing edge, respectively, was then determined as follows. The opposite wing margin was represented by a series of line segments connecting consecutive points entered along the wing margin, the last point being the far wing base, or the last entered point along the wing margin, if the far wing base was not visible. The slope and the z^*-intercept of the lines represented by each line segment were calculated. Beginning at the wing tip, the y^* value of the point of intersection of the line with slope s passing through P_7 and each consecutive line segment on the opposite wing margin was determined. If this value of y^* was intermediate to the two values of y^* of the points defining the line segment in question, this indicated a possible point of intersection P_8, with z_8^* being determined from the equation of the line connecting the two endpoints of the line segment. This procedure was carried out for each consecutive line segment on the opposite wing margin. For a particular point on the near wing margin, there were occasionally multiple points of intersection with the opposite wing margin. In these cases, the corresponding point P_8 was taken to be that point least distant in the y^*z^* plane from the last point of intersection that was found. This procedure for finding the corresponding point on the opposite wing margin was repeated for each point entered on the leading and trailing edges of the near wing.

At this stage, the x^* coordinates of both P_7 and P_8 are unknown; their difference can, however, be calculated from a knowledge of the direction number $\bar{a}^*$ in the (x^*,y^*,z^*) system as determined previously in the analysis of wing tip kinematics:

$$x_8^* = x_7^* - K_1\,, \tag{17}$$

where K_1 is equal to $\bar{a}^*(y_8^* - y_7^*)$. Several different methods were developed to calculate x_7^*, and the most accurate is given here: equating the distance between P_3 and P_7 to the distance between P_2 and P_8, and using equation 17, it is possible to solve for x_7^*:

$$x_7^* = [x_3^* - K_2 - (K_1 - x_2^*)^2]/2[K_1 - x_2^* + x_3^*]\,, \tag{18}$$

where

$$K_2 = (y_8^* - y_2^*)^2 + (z_8^* - z_2^*)^2 - (y_7^* - y_3^*)^2 - (z_7^* - z_3^*)^2\,.$$

Equation 18 was used to calculate the x^* coordinates of each point on the near wing margins. All points on the near leading and near trailing edges, as well as the near wing tip, were then transformed to the (x',y',z') system.

From the representation of the wing outline in the (x',y',z') system (Fig. 5A), the wing was then rotated to determine the three-dimensional location of chords equally spaced along the wing span. This system involves two sets of rotations from the insect coordinate system, such that the longitudinal axis of the wing is

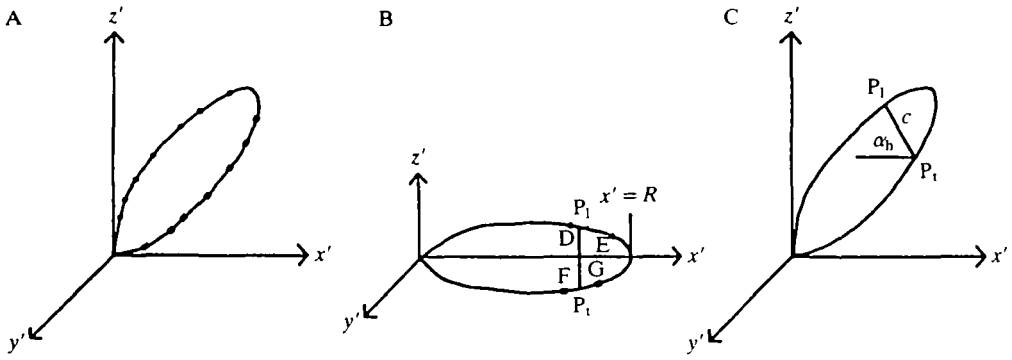

Fig. 5. (A) Representation of a wing in the (x',y',z') coordinate system. Circles are points on the leading edge of the wing, squares points on the trailing edge. (B) Rotation of the wing such that the longitudinal wing axis is coincident with the x' axis. One wing chord is shown, with endpoints P_l and P_t on the leading and trailing edge, respectively. (C) Wing in original orientation in the (x',y',z') system, depicting the angle α_h of the wing chord in B relative to horizontal. D–G, points on wing edges.

coincident with the x' axis. The points along the leading and trailing edges corresponding to the chords spaced at $0{\cdot}1R$ intervals, where R is wing length, along the wing span were then determined. For each such chord, the two closest data points D and E along the leading edge and F and G on the trailing edge of the wing were found (Fig. 5B). The y' and z' values of the two points of intersection of the chord with the leading and trailing edges were then determined by linear interpolation between the endpoints of the line segments $\overline{DE}$ and $\overline{FG}$, respectively. The nine pairs of span-wise points were then retransformed to the (x',y',z') system.

The angle α_h of a wing chord relative to the insect's horizontal is the complement of the angle between that chord and the axis z' (Fig. 5C). If points P_l and P_t denote the leading and trailing edge positions of the chord, respectively, this latter angle $\alpha_{z'}$ can be found from the following direction cosine:

$$\cos(\alpha_{z'}) = (z_l' - z_t')/c\,, \tag{19}$$

where c is the distance between P_l and P_t. Span-wise chord angles relative to horizontal were therefore determined by first calculating the three-dimensional distance between the corresponding points on the leading and trailing edges of the wing, and then solving for each span-wise chord $\alpha_{z'}$, as given by equation 19. The chord angle relative to horizontal, α_h, is taken to be, in degrees, $90-\alpha_{z'}$, positive angles referring to the condition when points on the leading edge of the wing are elevated (greater values of z') above points on the trailing edge.

Errors in the determination of the span-wise angle of attack were investigated by testing the analysis procedure on outlines of wing pairs drawn on a digital plotter (Houston Instruments DMP-6). The outlines were of approximately the same size as the magnified film image. The orientation of the insect relative to the viewing

system was approximately the same as that in the high-speed filming. The principal variables were investigated for the possible introduction of errors: positional angle of the wing, span-wise position of the chord, and projected chord length. Figures were drawn with constant span-wise angle of attack but differing positional angles of the wing, varying span-wise chord but constant span-wise angle of attack, and variable angle of attack along a wing of constant chord length. Typically 10 points were digitized along each wing margin, and the procedure was repeated five times to ascertain the precision of the analysis procedure. In general, the computer program returned the actual angle of attack to within 5°, with values being repeatable to within 3°. Systematic errors were least when the projected chord was smallest, and when chord lengths were relatively small. Therefore, no direct correlation existed between angle of attack or positional angle *per se* and the systematic errors associated with measuring the angle of attack. The sensitivity of the analysis program to errors in the calculated values of the direction cosines and the maximum projected wing length was also examined. Errors of up to 5 % in these parameters introduced errors in the measurement of angle of attack that were within the general limits of the systematic errors imposed by the procedure.

Morphology

To carry out an aerodynamic and energetic analysis of forward flight, it was necessary to determine a number of morphological parameters for those insects previously filmed. A detailed description of those morphological parameters relevant to flight has been given in Ellington (1984*a*). In particular, he has drawn attention to the significance of the moments of wing mass and wing area about the wing base, which reflect the distribution of mass and area along the wing span. Such moments, and their associated radii, are of immediate mechanical significance and, moreover, serve to characterize quantitatively the shape of the wing. A quasi-steady aerodynamic analysis of hovering flight (Weis-Fogh, 1973) demonstrated that the mean lift force and mean profile power are proportional to the second and third moments of wing area, respectively. Inertial forces acting on the wings are proportional to the first moment of mass; the associated radius through which the resultant force acts is the centre of mass. The second moment of mass is equivalent to the moment of inertia, its associated radius being the radius of gyration. Moments and radii analogous to those of wing mass can also be derived for the wing virtual mass, the mass of air accelerated and decelerated by the motion of the wing. Moments and radii of moments for wing area, mass and virtual mass will figure prominently in later calculations of lift and power requirements. The current morphological study follows for the most part Ellington's previously published methodology, which may be consulted for a more detailed description of the techniques and mathematical calculations involved.

The total mass m of the insect was first measured to $\pm 0{\cdot}1$ mg, and both wing pairs were then cut from the body. Wing length R and body length l_b were measured to within $\pm 0{\cdot}1$ mm using Vernier calipers. The non-dimensional body length $\hat{l}_b$ is given by the ratio of l_b to R. The legs were then cut

Table 1. *Identification (ID number and sex) and general morphological parameters for the bumblebees filmed for kinematic analysis*

ID	Sex	m (mg)	R (mm)	p_w ($N\,m^{-2}$)	$\mathcal{AR}$	$\hat{m}_t$
BB01	F (worker)	175	13·2	16·2	6·56	0·40
BB02	F (worker)	180	13·7	15·9	6·78	0·37
BB03	F (queen)	595	15·4	35·6	5·78	0·28

Body mass m is given in mg, wing length R in mm, and wing loading p_w in $N\,m^{-2}$. Aspect ratio $\mathcal{AR}$ and relative thoracic mass $\hat{m}_t$ are non-dimensional.

from the body, and the thorax was weighed. The ratio of thoracic mass to body mass is designated $\hat{m}_t$. For the insects filmed in free flight, gross morphological parameters as well as the aspect ratio $\mathcal{AR}$ of the wings and the wing loading p_w are given in Table 1. The aspect ratio is the ratio of the wing span squared to the wing area, and the wing loading is the ratio of body weight to wing area.

Body parameters

An entomological pin was put through the two wing bases and supported at either end such that the wing base axis was horizontal. A 35 mm photograph was then taken of the pinned body to determine the free body angle χ_0, the angle between the longitudinal body axis and horizontal. The body was then tapped and the period of oscillation about the wing base axis was determined. A 35 mm photograph was also taken of the insect body pinned through the abdomen and supported horizontally; superimposing this photograph with the previous one allowed a determination of the center of mass of the body. The distance from this center to the anterior tip of the body, when divided by the body length, is identified as $\hat{l}$, while the quantity $\hat{l}_1$ is the distance of the center of mass from the wing base axis, divided by the body length. The moment of inertia of the body I_b about the wing base axis could be calculated from the period of oscillation and $\hat{l}_1$, as could the radius of gyration for the moment of inertia $\hat{l}_2$. The insect body was then photographed both parallel and perpendicular to the longitudinal body axis, to determine the maximum projected area of the body in these two orientations ($S_{frontal}$ and S_{plan}). A non-dimensional mean body diameter, $\hat{d}$, was calculated from the formula:

$$\hat{d} = (4m/\pi\rho_b l_b^3)^{1/2}, \tag{20}$$

where the mean body density ρ_b was taken to be $1100\,kg\,m^{-3}$ (Ellington, 1984*a*). Morphological parameters for the bodies of those insects filmed in free flight are given in Table 2. A discussion of the passive pitching moments generated by the air flow about the body can be found in Dudley & Ellington (1990).

Wing parameters

One wing pair was mounted between glass slides and used as a negative in a

Table 2. *Body parameters for filmed bumblebees*

ID	$\hat{l}_b$	$\hat{l}$	$\hat{l}_1$	$\hat{l}_2$	χ_0 (degrees)	I_b (10^{-9} kgm^2)	$\hat{d}$
BB01	1·41	0·48	0·21	0·28	57·5	0·49	0·18
BB02	1·38	0·43	0·21	0·31	58·5	0·58	0·19
BB03	1·45	0·53	0·27	0·36	53·6	3·97	0·25

Free body angle χ_0 is given in degrees, moment of inertia I_b of the body about the wing base axis in 10^{-9} kgm^2.

The non-dimensional parameters are explained in the text.

photographic enlarger to obtain a positive print. Using the same equipment as in the kinematic analysis, approximately 20 points along the leading and along the trailing edge of the wing were digitized. A cubic spline function was then fitted to each wing edge, and values of the wing chord c were determined for 100 equally spaced intervals along the wing span. Wing area S was calculated, as was a normalized mean wing chord. The first and second moments of wing area S_1 and S_2 were then calculated from:

$$S_k = 2\int_0^R cr^k \mathrm{d}r\,, \tag{21}$$

for k equal to 1 and 2, respectively. The variable r is the distance from the wing base of a strip of wing area dS. The corresponding non-dimensional radii for the moments of wing area, $\hat{r}_1(S)$ and $\hat{r}_2(S)$ were determined from:

$$\hat{r}_k{}^k(S) = S_k/SR^k\,. \tag{22}$$

The mass of the other wing pair was first determined to $\pm 1\,\mu$g; the wing mass m_w includes both wing pairs. A strip weighing technique was then used to determine the span-wise mass distribution. Consecutive 2 mm wide strips were cut from the wing, perpendicular to the longitudinal wing axis, and sequentially from the basal hinge line to the wing tip. The mass of each strip was measured to $\pm 0{\cdot}5\,\mu$g using a Kahn no. 1500 electrobalance. The first (m_1) and second (m_2) moments of wing mass were calculated from the following formula, for k equalling 1 and 2, respectively:

$$m_k = 2\int_0^R m' r^k \mathrm{d}r\,, \tag{23}$$

where m' is the mass per unit wing length. The corresponding non-dimensional radii for the moments of wing mass, $\hat{r}_1(m)$ and $\hat{r}_2(m)$ are given by:

$$\hat{r}_k{}^k(m) = m_k/m_w R^k\,. \tag{24}$$

Because of weight loss from the wing during the cutting procedure, calculated values of m_k were multiplied by the ratio of the initial wing mass to the sum of the

Table 3. *Non-dimensional wing parameters for filmed bumblebees*

ID	$\hat{r}_1(m)$	$\hat{r}_2(m)$	$\hat{r}_1(S)$	$\hat{r}_2(S)$	$\hat{r}_1(v)$	$\hat{r}_2(v)$	$\hat{v}$	$\hat{h}$ (%)	$\hat{m}_w$ (%)
BB01	0·38	0·46	0·495	0·554	0·496	0·542	1·09	0·054	0·52
BB02	0·35	0·42	0·483	0·540	0·473	0·518	1·12	0·054	0·47
BB03	0·38	0·45	0·491	0·553	0·487	0·538	1·07	0·063	0·32

The abbreviations are defined in the Appendix.

masses of the individual wing strips (Ellington, 1984*a*). A mean wing thickness relative to wing length, $\hat{h}$, was calculated from the formula:

$$\hat{h} = m_w/\rho_w SR\,, \tag{25}$$

the density of the wing ρ_w taken as $1200\,kg\,m^{-3}$, the density of solid cuticle (Wainwright *et al.* 1976).

Mechanically analogous to the wing mass is the wing virtual mass, the mass of air set into motion by the acceleration of a wing normal to its chord, as is typical of the wings at the end of half-strokes. The virtual mass of the wing pair, v, is given by:

$$v = 2\int_0^R V'dr\,, \tag{26}$$

where v' is the virtual mass per unit wing length, equal to $\rho\pi c^2/4$, and ρ is the density of air. A non-dimensional virtual mass $\hat{v}$ can be calculated from:

$$\hat{v} = v\mathcal{A}R^2/2\pi\rho R^3\,. \tag{27}$$

The first and second moments of wing virtual mass are calculated as in equation 23, substituting v' for m'. The non-dimensional radii for moments of virtual mass are similarly calculated using equation 24 and the moments of virtual mass. Non-dimensional wing parameters for filmed insects are given in Table 3.

Results

General flight performance

Bumblebees in the working section of the tunnel usually took off and flew upwards within seconds of the ultraviolet light being turned on. The strength of this response could be varied by adjusting the light intensity. If the striped drums were not rotating, the flight was quite erratic with no consistent orientation, the insect frequently flying into the sides of the working section. When the drums were rotating, however, insects generally took 1–2 s to 'lock on' to the moving stripes and begin steady forward flight. In such flight, the insect rarely moved more than three body lengths from some mean position in the working section. Control of flight was excellent, and only rarely was steady flight interrupted by periods of instability from which the insect generally recovered within 1 s. Continuous steady flights sometimes lasted up to 1·5 min. Surprisingly, no strong correlation was observed between the rate of rotation of the striped drums and the flight velocity

of the insect; flight at 4·5 m s^{-1} could sometimes be maintained at a very low drum rotation rate. At a particular flight speed, however, it was possible suddenly to increase the drum speed, and thereby elicit short-term movement of the insect forward in the tunnel. Simply by reversing the apparent stripe motion on the drums relative to the direction of the wind, it was also possible to induce backwards flight over the entire speed range. Bumblebees upon occasion exhibited remarkable feats of maneuverability. In one instance a bumblebee worker took off backwards from the back netting of the working section, flew backwards for several seconds, then rotated precisely about the vertical axis by 180°, and flew forwards. This feat was accomplished at an airspeed of 4·5 m s^{-1}.

When the lights for filming were turned on, insects generally continued flying for up to 1 s before becoming disoriented by the intense lights and subsequently landing. Visual observation indicated that flight in the fraction of a second the insects were actually being filmed was stable, unaccelerated flight. Only those films which showed properly oriented flight, as shown by minimal roll from the vertical and yaw from the oncoming wind, were chosen for the kinematic analysis. Three series of bumblebee films were analyzed in detail. Each series consisted of four films of a particular bumblebee flying at the three aforementioned forward airspeeds and while hovering. For one insect, the bumblebee queen (BB03), no good quality flight was observed at 4·5 m s^{-1}, and this speed is therefore omitted in the results for this insect.

Table 4 shows for each analyzed film the roll from vertical and yaw from the tunnel of the insect during the analyzed wingbeat. The yaw value in hovering flight is, of course, of no particular importance. Also given in Table 4 is the advance ratio, J, at each flight speed. The advance ratio is the ratio of the flight velocity to the mean flapping velocity of the wings, and can be defined as (Ellington, 1984*b*):

$$J = V/(2\Phi nR), \tag{28}$$

Table 4. *Advance ratio* J, *roll and yaw angles to the nearest degree, and Reynolds number* Re *for bumblebees filmed in free flight*

ID	V (m s^{-1})	J	Roll (degrees)	Yaw (degrees)	Re (body)	Re (wing)
BB01	4·5	0·66	26	10	5580	2990
	2·5	0·28	16	−3	3100	1940
	1·0	0·13	19	7	1240	1360
	Hover	–	20	14	–	1210
BB02	4·5	0·59	16	5	5670	2120
	2·5	0·34	21	−10	3150	1760
	1·0	0·16	14	−19	1260	1200
	Hover	–	15	−2	–	1080
BB03	2·5	0·34	8	−9	3720	2890
	1·0	0·09	15	1	1490	2230
	Hover	–	8	−8	–	2030

where Φ is the stroke amplitude, n the wingbeat frequency, and R the wing length. The flight velocity V is taken to be the airspeed in the tunnel, and therefore ignores small deviations in the insect's flight speed. An arbitrary limit to J for hovering flight is 0·1 (Ellington, 1984*b*), and for all the hovering sequences movement of the wing base was less than that imposed by this limit. Precise determination of the velocities of insects in hovering flight was not possible because the camera view precluded accurate determination of the x' coordinates of points on the body. It should be noted that the advance ratio of the bumblebee queen flying at $1\,m\,s^{-1}$ is less than the value taken to represent hovering flight. Table 4 also includes, for flight at each airspeed, two values of the Reynolds number, one based on the body length and forward airspeed, the other based on the mean wing chord and the sum of the forward airspeed and the mean flapping velocity at the radius of the second moment of wing area. This latter quantity is meant only to give a general indication of the flow situation, as there is, of course, continuous variation of the Reynolds number both along the wing and during the wingbeat.

Wing tip and body kinematics

Fig. 6 shows the variation with airspeed of the body angle χ and the stroke plane angle β. Body angle invariably decreased with forward airspeed; the stroke plane concomitantly increased, with the angle between the stroke plane and the longitudinal body axis remaining approximately constant for any particular insect. Fig. 7 shows the variation with airspeed of the following kinematic parameters: the minimum positional angle, ϕ_{min}, mean positional angle, $\bar{\phi}$, maximum positional angle, ϕ_{max}, stroke amplitude, Φ $(=\phi_{max}-\phi_{min})$, and the wingbeat frequency, n. There was no statistically significant change with airspeed in minimum positional

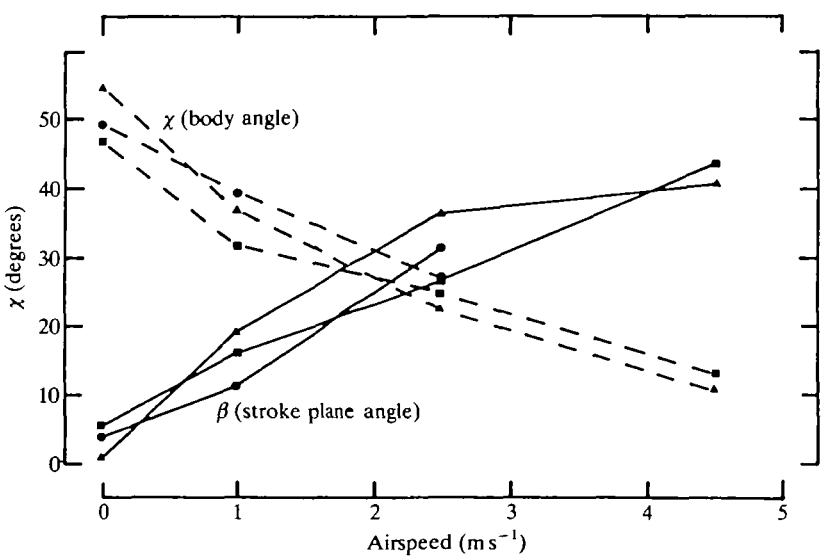

Fig. 6. The variation with airspeed of the body angle χ and the stroke plane angle β. Symbols as follows: ■, BB01; ▲, BB02; ●, BB03.

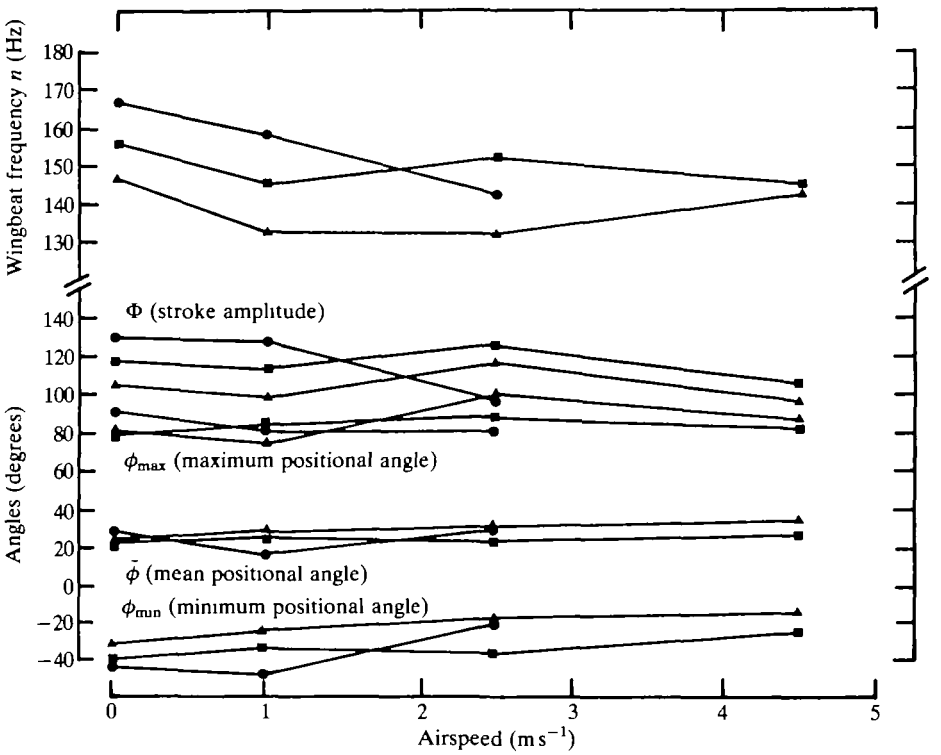

Fig. 7. The variation with airspeed of the wingbeat frequency n, the stroke amplitude Φ, the maximum positional angle ϕ_{max}, the mean positional angle $\bar{\phi}$ and the minimum positional angle ϕ_{min}. Symbols as in Fig. 6.

angle, mean positional angle, maximal positional angle or stroke amplitude; slopes of linear regressions relating these quantities to airspeed were in no case significantly different from zero ($P > 0{\cdot}05$). Similarly, no consistent trend characterized the relationship between wingbeat frequency and airspeed ($P > 0{\cdot}05$). Frequency measurements were also made on a large number of films that were not analyzed for detailed kinematics; wingbeat frequency was independent of airspeed, for insects ranging in body mass from 150 to 595 mg. No consistent relationship was found between wingbeat frequency and body mass at any forward airspeed or for hovering flight. Insects of a similar mass often differed in wingbeat frequency by 20–30 Hz.

Detailed wing tip kinematics

Detailed wing tip kinematics for each airspeed and hovering flight are given in Figs 8–10. On the right side of each figure is depicted the variation of the positional angle ϕ with non-dimensional time $\hat{t}$ ($=nt$); the wingbeat frequency is also given. The open circle on each graph corresponds to the frame of maximum projected length, where errors in the projection analysis will be greatest. The diagrams on the left-hand side of Figs 8–10 depict the wing tip path relative to the

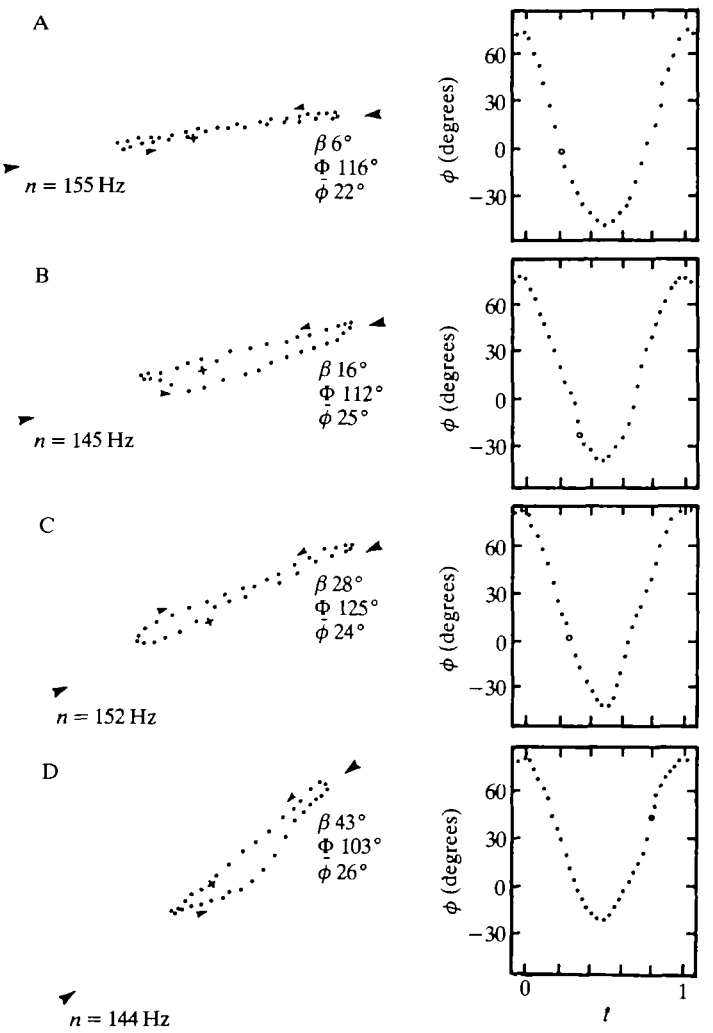

Fig. 8. Wing tip kinematics for the insect BB01. (A) Hovering; (B) $1\,m\,s^{-1}$; (C) $2{\cdot}5\,m\,s^{-1}$; (D) $4{\cdot}5\,m\,s^{-1}$. Symbols as follows: n, wingbeat frequency; β, stroke plane angle; Φ, stroke amplitude; $\bar{\phi}$, mean positional angle; ϕ, positional angle; t, non-dimensional time; open circle, the frame of maximum projected length; cross, wing base. See text for further details.

stroke plane, the wing base being indicated by a cross. The positional angle ϕ equals 0° at the wing base, and ±90° at the tips of the large arrowheads. The elevational angle θ can be read off an identically scaled axis perpendicular to the stroke plane and passing through the wing base. The small arrowheads indicate the separate paths of the downstroke and upstroke. For each wing tip path, the stroke plane angle, β, stroke amplitude, Φ, and mean positional angle, $\bar{\phi}$, are also given in degrees.

From the graphs of positional angle *versus* non-dimensional time, non-

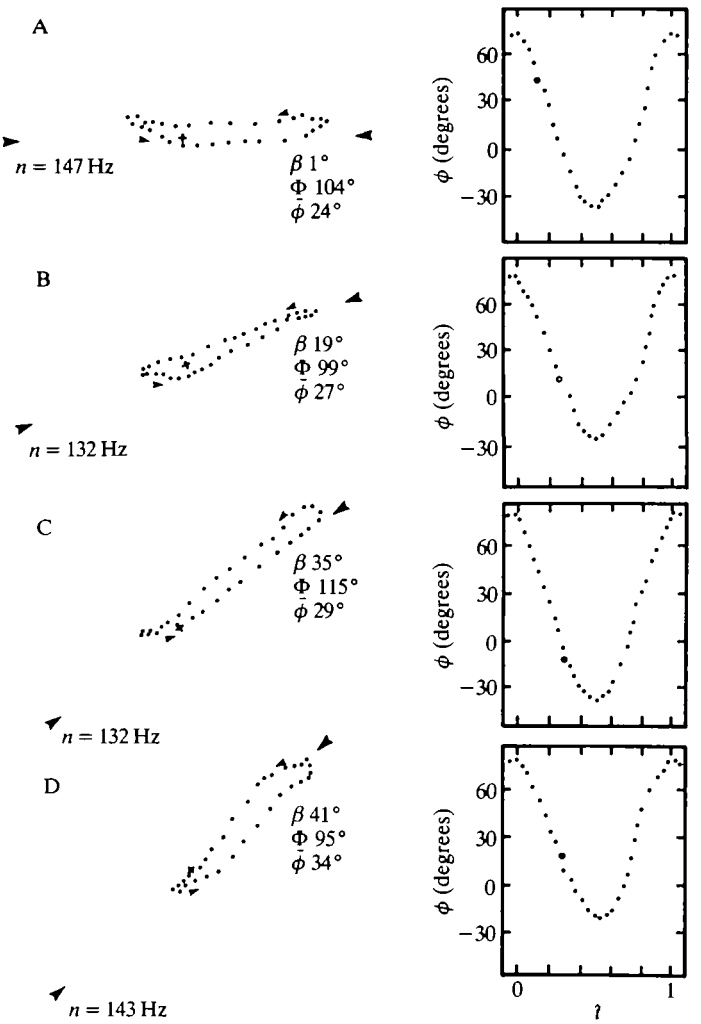

Fig. 9. Wing tip kinematics for the insect BB02. (A) Hovering; (B) $1\,m\,s^{-1}$; (C) $2{\cdot}5\,m\,s^{-1}$; (D) $4{\cdot}5\,m\,s^{-1}$. Symbols as in Fig. 8. See text for further details.

dimensional angular velocities were calculated according to Ellington (1984*b*). Root mean square (rms) and cube root mean cube (crmc) values were calculated for each wingbeat. No relationship was found between the rms or crmc values and forward airspeed (r typically 0·1, $P > 0{\cdot}05$). Additionally, no relationship was found between forward airspeed and the ratio of the rms value during the downstroke to that during the upstroke ($r = -0{\cdot}21$, $P > 0{\cdot}05$). Values of rms and crmc were only 1–2 % smaller than the values characterizing simple harmonic motion. Corresponding estimates of quasi-steady aerodynamic forces and mean profile power are about 5 % lower than estimates based on the assumption of

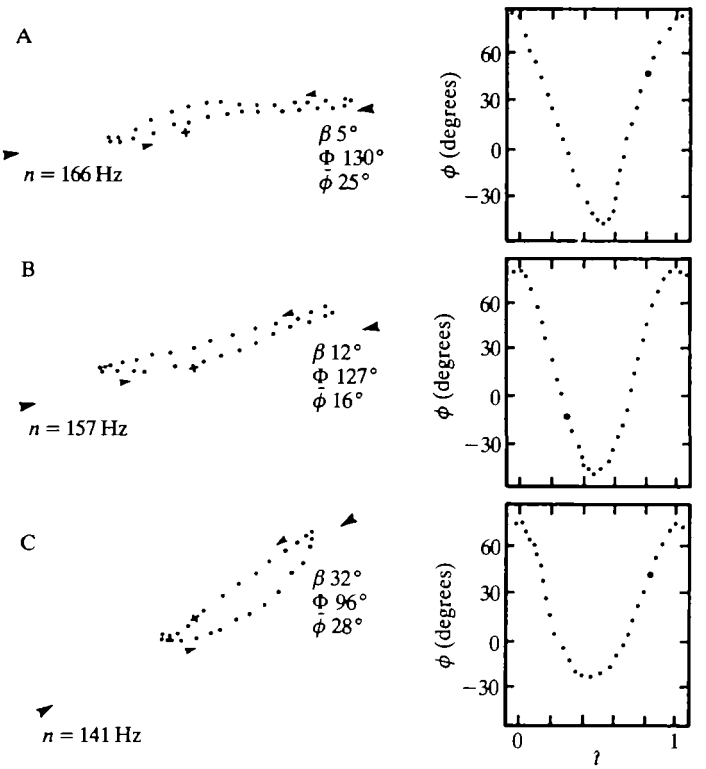

Fig. 10. Wing tip kinematics for the insect BB03. (A) Hovering; (B) $1\,m\,s^{-1}$; (C) $2{\cdot}5\,m\,s^{-1}$; (D) $4{\cdot}5\,m\,s^{-1}$. Symbols as in Fig. 8. See text for further details. Insect did not fly at $4{\cdot}5\,m\,s^{-1}$.

simple harmonic motion for the wings. Durations of the downstroke and of the upstroke were determined from the graphs of positional angle *versus* non-dimensional time; no correlation was found between the ratio of the downstroke to upstroke and forward airspeed ($r = -0{\cdot}28$, $P > 0{\cdot}05$). This ratio averaged 1·06 (S.D. 0·08) for the bumblebee sequences analyzed.

Wing tip paths generally were open loops with the downstroke dorsal to the upstroke. Several sequences showed single crossovers, either in the middle or at the end of the wingbeat. No double crossovers were observed. Curves were drawn by eye through the plots of positional angle *versus* elevational angle; mean values of the elevational angle were calculated for the downstroke and upstroke. The difference between these values, $|\Delta\bar{\theta}|$, was determined, as was the maximum difference $|\Delta\theta_{max}|$ between the mean elevational angle of the downstroke and that of the upstroke at any particular value of ϕ. The two parameters $|\Delta\bar{\theta}|$ and $|\Delta\theta_{max}|$ give an indication of the divergence of the wing tip path from the stroke plane. Both the quantities $|\Delta\bar{\theta}|$ and $|\Delta\theta_{max}|$ tended to be positively correlated with airspeed ($r = 0{\cdot}06$, $P < 0{\cdot}05$). The maximum observed value of $|\Delta\theta_{max}|$ was approximately 16°, indicating that, in spite of the aforementioned trend of a more

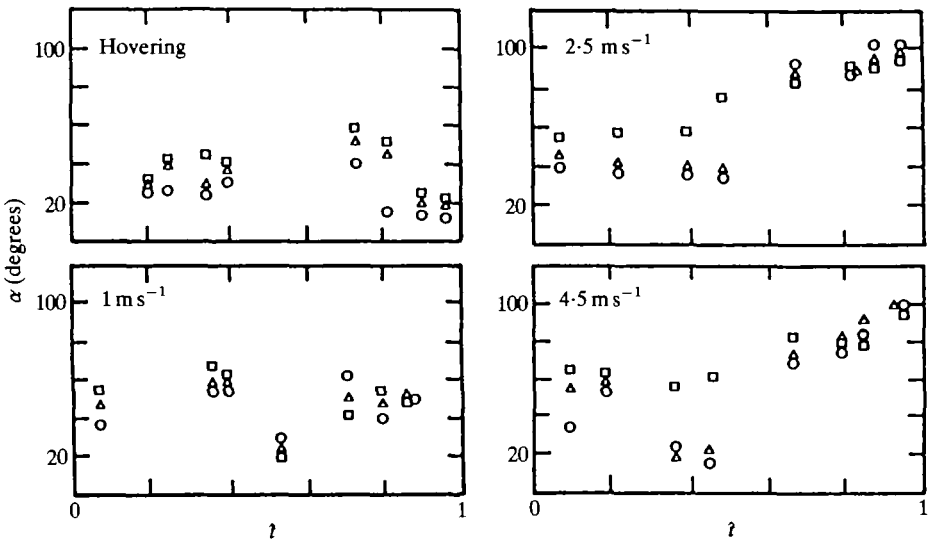

Fig. 11. Variation with non-dimensional time t of the angle of attack α relative to the stroke plane, for the insect BB01. Symbols as follows: □, proximal wing section, the mean angle of wing chords at $0{\cdot}1R$, $0{\cdot}2R$ and $0{\cdot}3R$; △, middle section, the mean angle of wing chords at $0{\cdot}4R$, $0{\cdot}5R$ and $0{\cdot}6R$; ○, distal section, the mean angle of wing chords at $0{\cdot}7R$, $0{\cdot}8R$ and $0{\cdot}9R$, where R is wing length.

dorsal downstroke, wing motion is generally confined to the stroke plane at all airspeeds.

Span-wise angle of attack

Figs 11–13 depict geometrical angles of attack α relative to the stroke plane as a function of non-dimensional time for the analyzed bumblebee sequences. Although the initial analysis of angle of attack determined chord angles relative to horizontal, angles of attack relative to the stroke plane are, in general, more informative and are presented here. Use of the phrase 'angle of attack' henceforth refers to the geometrical angle of attack. Values of α are given for three consecutive sections along the wing span, and represent the mean angle of the three chords comprising each section. Each data point is the mean of three separate determinations from a film image of the span-wise angle of attack. The analysis program proved to be particularly inaccurate when the margins of opposite wings were parallel to one another; the determination of corresponding points on the wing margins was then very sensitive to digitizing errors. Hence frames in the middle of a half-stroke (ϕ near zero) were difficult to analyze, and most frames analyzed were near the onset or finish of rotation at the ends of half-strokes. Particularly near the wing base, the resolution of the wing margins was poor, and angles of attack for the proximal section are therefore not as accurate as those for the two more distal sections.

Angles of attack during both the downstroke and the upstroke tended to

increase with increased airspeed, although there were a few exceptions to this trend. Angles of attack were generally constant to within 15° during the periods between wing rotation, although, particularly during the upstroke, a number of sequences displayed continuously increasing or continuously decreasing angles of attack. During the downstroke, bumblebee wings were typically twisted along the

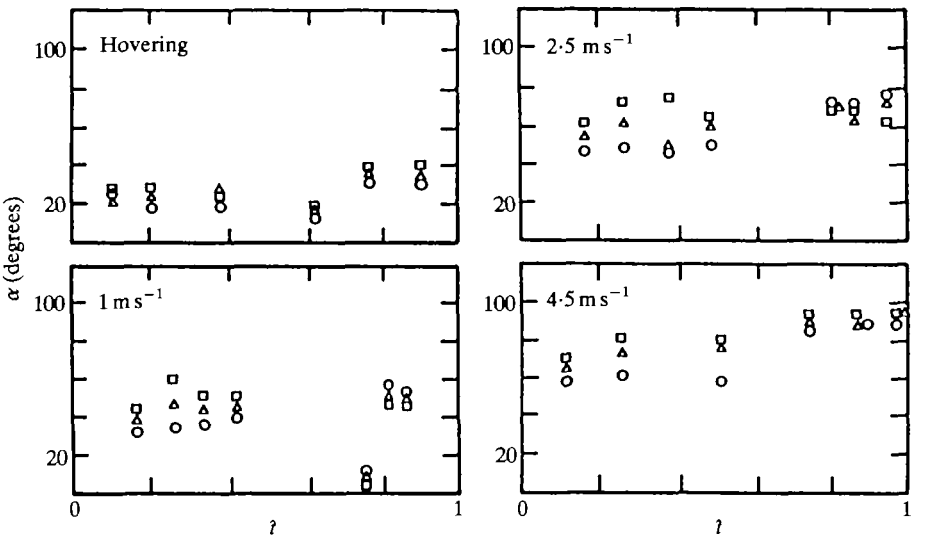

Fig. 12. Variation with non-dimensional time t of the angle of attack α relative to the stroke plane, for the insect BB02. Symbols as in Fig. 11.

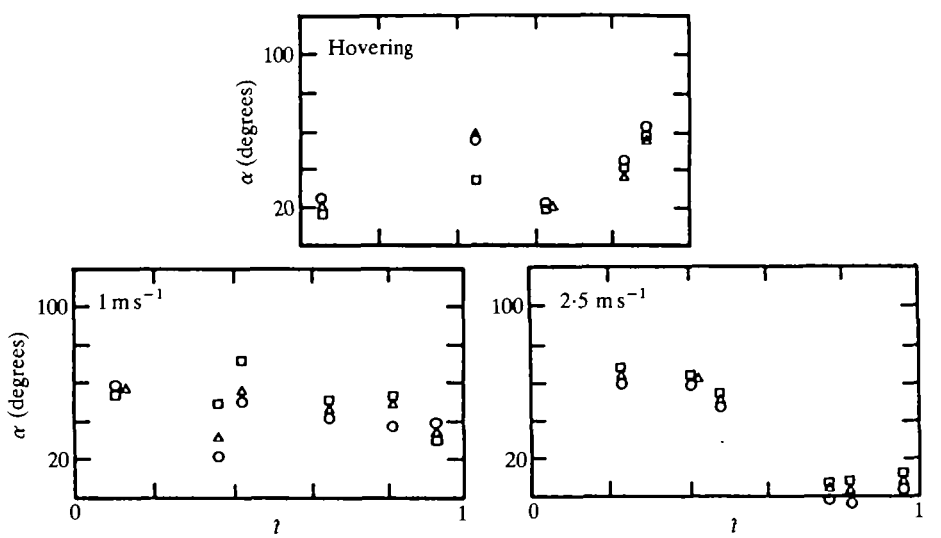

Fig. 13. Variation with non-dimensional time t of the angle of attack α relative to the stroke plane, for the insect BB03. Symbols as in Fig. 11. There was no flight at $4{\cdot}5\,m\,s^{-1}$.

wing span by 10–20°, approximately the same amount as is observed under static conditions. Wings were cambered during the downstroke, and for flight at the higher airspeeds remained so during the upstroke; the extent of wing cambering during the upstroke for flight at $1\,m\,s^{-1}$ and for hovering flight was difficult to ascertain.

At the ends of half-strokes the wings increased their angle of attack, rotating about the longitudinal axis to the angle of attack characteristic of the following half-stroke. Nose-down rotation of the wing is pronation, whereas nose-up rotation is supination. The exact timing of wing rotation was difficult to determine. Particularly at the end of either pronation or supination the termination of wing rotation was difficult to specify precisely, and the time chosen to indicate the end of wing rotation was that point after which no more elastic recoil was apparent. Similarly, the onset of wing rotation usually occurred between film frames, with consequent loss of temporal resolution. Measurements of the timing of wing rotations can therefore only be regarded as approximate. The durations of pronation and supination were approximately equal, averaging about 22 % of the wingbeat period. No relationship was found between forward airspeed and the duration of pronation or supination (r typically $-0{\cdot}35$, $P>0{\cdot}05$), and no consistent relationship was found between the onset of pronation or supination and the top or bottom, respectively, of the wingbeat (r typically $-0{\cdot}2$, $P>0{\cdot}05$).

Mean angles of wing rotation at the ends of half-strokes were determined by taking the mean of the angle of rotation for the nine equally spaced span-wise chords. These angles tended to decrease with increased airspeed for both pronation ($r=-0{\cdot}67$, $P<0{\cdot}05$) and supination ($r=-0{\cdot}75$, $P<0{\cdot}05$). A non-dimensional form of wing rotation $\hat{\omega}$, equal to the mean angular velocity of rotation divided by the wingbeat frequency, represents the angle through which the wing would rotate over an entire wingbeat (Ellington, 1984*b*). The variation with airspeed of this quantity is given in Fig. 14; for both pronation and supination, $\hat{\omega}$ tended to decrease with increased airspeed (pronation: $r=-0{\cdot}50$, $P<0{\cdot}05$; supination: $r=-0{\cdot}76$, $P<0{\cdot}05$).

During wing rotation, significant changes in wing profile were observed. The anterior region of the wing first began to rotate as a unit, and was followed by rotation of the posterior region, as described by Ellington (1984*b*) for insects in hovering flight. Rotation of the posterior region was always manifested as a torsional wave moving towards the wing base and never towards the wing tip. Wings usually rotated past the angle of attack characterizing the following half-stroke, and then recoiled back to this angle. Profile flexion of the wings was most pronounced in hovering flight, and decreased progressively as flight speed increased; recoil of the wing after rotation was similarly reduced at higher airspeeds.

Discussion

Forward flight in animals requires, in addition to the support of body weight, the

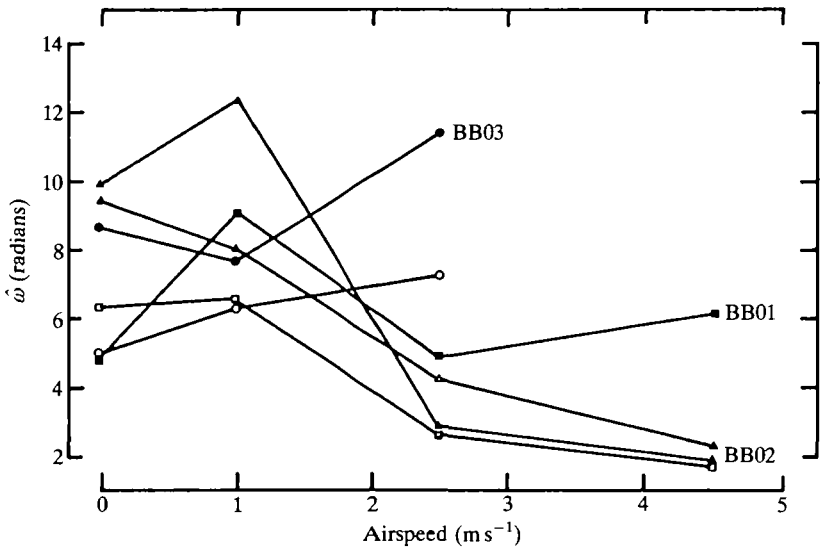

Fig. 14. Variation with airspeed of angular velocity of rotation $\hat{\omega}$ during pronation and supination. Symbols as in Fig. 6; open symbols refer to wing pronation, closed symbols to wing supination.

generation of thrust to overcome body drag. Thrust is the net horizontal component of the total forces generated by the wing during the wingbeat. As forward airspeed increases, the magnitude of this horizontal component must increase to offset the additional body drag, while the net vertical force produced must continue to equal the body mass (less any lift on the body). Typically, in flying insects the ratio of drag to body weight is small, even at high airspeeds, and the resultant force vector tilts forwards only by several degrees. This small change can be contrasted with the large change in body angle and stroke plane angle over the same airspeed range. A strong correlation between flight speed and body angle has been observed in flying insects (*Drosophila*: Vogel, 1966; Götz, 1968; David, 1979; honeybee: Nachtigall *et al.* 1971; Esch *et al.* 1975; bumblebees: present study) and birds (Brown, 1953; Greenewalt, 1960; Pennycuick, 1968; Rüppell, 1971). The angle between the stroke plane and the longitudinal body axis is relatively constant, and the gradual decrease in body angle with forward airspeed is paralleled by a concomitant increase in stroke plane angle (Ellington, 1984*b*).

What are the consequences for the magnitude and direction of aerodynamic forces of the increase in airspeed and the tilt of the stroke plane? By using the parameter of the advance ratio J ($= V/2\Phi nR$), it is possible to evaluate the consequences for forward flight. For acute stroke plane angles, an increase in the advance ratio will result in the forces generated by the wing during the downstroke and the upstroke becoming increasingly asymmetrical (Ellington, 1984*b*). The relative velocity during the downstroke becomes greater than that during the

upstroke, with a concomitant increase in the magnitude of aerodynamic forces, and the downstroke becomes progressively more horizontal while the upstroke becomes more vertical, with a corresponding change in the direction of the resultant aerodynamic force. These changes are mitigated only partially by the increase in stroke plane angle, which tends to decrease the velocity differences between the half-strokes. In bats and birds the asymmetry between half-strokes can be enhanced by changes in wing profile which considerably reduce the magnitude of aerodynamic forces produced during the upstroke. Insects, however, cannot drastically alter wing shape during the wingbeat, apart from transverse flexion at the ends of half-strokes and changes in wing camber.

Because the advance ratio is inversely proportional to the wingbeat frequency and to the stroke amplitude, variation in these kinematic parameters will alter the magnitude and direction of aerodynamic forces produced by the wings. An increase in either the wingbeat frequency or the stroke amplitude while the other parameter is constant will increase the flapping velocity of the wings, with consequent changes in the relative velocity experienced by a wing section. Because lift and drag forces are, in general, proportional to the square of the relative velocity, the magnitudes of the resulting aerodynamic forces will change disproportionately. For this reason, considerable attention has been given to the variation with airspeed of the wingbeat frequency and the stroke amplitude.

For the buff-tailed bumblebees of the present study, no systematic change in wingbeat frequency with airspeed was observed. For various insects, bats and birds, a number of studies have demonstrated alternatively an increase, no change or a decrease in wingbeat frequency as forward airspeed increases. Sotovalta (1947) reported for a hoverfly (*Eristalis arbustorum*) that wingbeat frequency in free flight increased approximately from 260 Hz to 275 Hz over a flight speed range of hovering to 5 m s^{-1}, while for *Calliphora* the increase was from 120 Hz to 210 Hz over a range of 0·5 to 5 m s^{-1}. In free-flying *Locusta migratoria*, there is a positive correlation between flight speed and wingbeat frequency, albeit with considerable scatter in the data (Baker *et al.* 1981). This relationship has also been found in tethered migratory locusts (Gewecke; 1975). In the long-eared bat *Plecotus auritus* wingbeat frequencies showed a small decrease over the speed range 2–3 m s^{-1} (Norberg, 1976), while for the bat *Myotis lucifugus* wingbeat frequency decreased from approximately 16 Hz at a flight speed of 2 m s^{-1} to a value of 10 Hz at 7 m s^{-1} (Schnitzler, 1971). Carpenter (1985) found that in the flying fox *Pteropus poliocephalus* the wingbeat frequency decreased by a factor of 2 over the range 3–7 m s^{-1}, and then increased at higher airspeeds. Aldridge (1986) showed for the greater horseshoe bat *Rhinolophus ferrumequinum* that wingbeat frequency decreased with increased airspeed. Tucker (1966) found for a free-flying budgerigar *Melopsittacus undulatus* that wingbeat frequency varied by less than 6 % from the mean value over a speed range 5–9 m s^{-1}, while Schnell (1974) found for the magnificent frigatebird *Fregata magnificens* no significant correlation between flight speed and wingbeat frequency over the range 8–14 m s^{-1}. In a study of flight mechanics of *Columba livia*, Pennycuick (1968) found a decrease in wingbeat

frequency as flight speed increased from 7 to 13 $m\,s^{-1}$, followed by a slight increase at higher airspeeds. A similar pattern was found for the stroke amplitude, although for both kinematic parameters scatter in the data was considerable. McGahan (1973) found no significant correlation between forward airspeed and wingbeat frequency in the Andean condor *Vultur gryphus*, but it is not clear whether these measurements were made on the same individuals at different airspeeds. Butler & Woakes (1980) found no relationship between wingbeat frequency and airspeed for barnacle geese (*Branta leucopsis*); wingbeat frequency was approximately constant over a speed range of 16–24 $m\,s^{-1}$. The variable consequences of changes in airspeed for the wingbeat frequency of flying animals suggests, not surprisingly, that considerable diversity exists in the aerodynamic mechanisms used by animals of widely varying shapes and sizes to effect forward flight.

As with wingbeat frequency, the stroke amplitude of buff-tailed bumblebees in free flight showed no significant change with airspeed. A wide diversity of changes in stroke amplitude with airspeed has been observed in flying animals. Magnan (1934) noted in free-flying insects a general decrease in stroke amplitude with increased airspeed. Gewecke (1967, 1970, 1974) has documented for tethered *Calliphora*, *Locusta* and the dragonfly *Orthetrum* a significant decrease in stroke amplitude with increased airspeed. Hollick (1940) noticed in tethered individuals of the fly *Muscina stabulans* a decrease in stroke amplitude with increased airspeed, as well as with decreased body inclination relative to horizontal. Urquhart (1960), apparently on the basis of a visual estimate in the field, reported that in cruising flight of the monarch butterfly *Danaus plexippus* the stroke amplitude was only 30°, but that the amplitude while in 'speeding flight' increased to 120°. Sotovalta (1947) suggested that the stroke amplitude in slow forward flight of the sphingid *Sphinx ligustri* increased from the value in hovering flight, without a significant change in wingbeat frequency. In the long-eared bat *Plecotus auritus* the stroke amplitude while hovering was 120°, which decreased to 91° at a flight speed of approximately 2·4 $m\,s^{-1}$ (Norberg, 1976). Reviewing these results, it is clear that no consistent relationship between stroke amplitude and airspeed has been observed for flying animals, and perhaps none should be expected, given again the morphological diversity of the animals being considered.

Given that neither wingbeat frequency nor stroke amplitude vary with airspeed for flying bumblebees, the mechanism by which changes in body angle and stroke plane angle are effected are not clear. An increase in the mean positional angle with airspeed will move the center of lift progressively more dorsally, and could therefore provide the nose-down pitching moment necessary to tilt the body, and hence the resultant force vector, to the angles characteristic of forward flight (Ellington, 1984*b*). Nose-down pitching moments required from the wings to produce the appropriate body angles are at all airspeeds greater than zero (Dudley & Ellington, 1989). No such increase in mean positional angle with airspeed was apparent in this study. It should be noted that pitching moments about the wing base axis, as predicted by a quasi-steady aerodynamic analysis, are not simply

proportional to the mean positional angle but are also inversely proportional to the stroke plane angle (Dudley & Ellington, 1990).

The high-speed cinematographic studies described herein of bumblebees in free flight have revealed no systematic variation with airspeed of wingbeat frequency, stroke amplitude or minimum, mean or maximum positional angle over the range of airspeeds from hovering to $4{\cdot}5\,m\,s^{-1}$. Instantaneous values of these kinematic parameters at any given airspeed were, however, found for bumblebees to deviate considerably from mean values for flights of several minutes. If such temporal variation in kinematics is typical of insects in free flight, the kinematic parameters obtained from a single high-speed film covering a very short time period may not necessarily be representative of mean values. Multiple high-speed films of the same insect flying at a constant airspeed would address this issue.

The remaining kinematic parameter to be discussed is the angle of attack of the wing. While drastic changes in wing profile cannot be used to create an asymmetry between the downstroke and upstroke, changing the angle of attack of the wing relative to the stroke plane (Figs 11–13) can be used to control the production of thrust and, thereby, to regulate forward airspeed. Such changes in the angle of attack are easily made by altering the extent of wing rotation at the ends of half-strokes (Fig. 14), which may be controlled by the activity of only one muscle or muscle group involved in rotation. Because wing orientation changes gradually with airspeed, the increase in asymmetry between the downstroke and upstroke should also be gradual, as will be shown using a quasi-steady aerodynamic analysis for bumblebees in free forward flight (Dudley & Ellington, 1990).

The hypothesis that asymmetry between the downstroke and upstroke, and hence variable production of thrust, results from changes in wing orientation is supported by considering the direction of forces produced on the wing, as determined by the effective angles of incidence. The effective angle of incidence is measured from the relative velocity vector, which is the sum of the forward, flapping and induced velocities. Calculations of the effective angles of incidence for bumblebees in forward flight will be made in the companion paper (Dudley & Ellington, 1990), where it will be shown that effective angles of incidence are independent of airspeed, and do not change significantly from the downstroke to the upstroke. Because the stroke plane angle varies with airspeed, therefore, the direction of forces produced by the downstroke and upstroke must also change as a function of airspeed. In hovering flight with a horizontal stroke plane, the upstroke and downstroke contribute equally to the production of vertical forces, but as airspeed increases the downstroke contributes progressively more and the upstroke less to sustaining the body weight. At higher airspeeds the upstroke functions primarily to generate thrust, which arises from lift forces on the wing.

In conclusion, bumblebees in forward flight use changes in the angle of attack of the wing relative to the stroke plane to generate a force asymmetry between the downstroke and upstroke, and hence to regulate forward airspeed. Effective angles of incidence remain constant during the downstroke and upstroke; because

of wing rotation, the sense of wing circulation is reversed. The consequences for force production are a progressive change in the direction of the lift and drag, with the vertical forces increasing in magnitude during the downstroke and the horizontal forces increasing during the upstroke. The gradual change in wing orientation during the downstroke and upstroke corresponds to the gradual change in the asymmetry between half-strokes required to offset the additional body drag at higher airspeeds.

Appendix

a^*	x^* direction number of line connecting the wing tips in the (x^*,y^*,z^*) coordinate system
$\bar{a}^*$	Mean value of a^*
A	Reference area for force coefficient
A_0	Area of actuator disc
AR	Aspect ratio
B	Wing base separation
c^*	z^* direction number of line connecting the wing tips in the (x^*,y^*,z^*) coordinate sytem
$\bar{c}^*$	Mean value of c^*
c	Wing chord
C_D	Drag coefficient
$\overline{C}_D$	Mean drag coefficient
$C_{D,f}$	Drag coefficient for a flat plate parallel to flow
$C_{D,ind}$	Induced drag coefficient
$C_{D,pro}$	Profile drag coefficient
C_L	Lift coefficient
$C_{L,max}$	Maximum lift coefficient
$\overline{C}_L$	Mean lift coefficient
$\hat{d}$	Mean body diameter/body length
D	Drag
D_b	Body drag
F	Total force acting on insect body
F_{hor}	Horizontal force acting on body
F_{vert}	Vertical force acting on body
$F_{vert,d}$	Vertical force produced during downstroke
g	Gravitational acceleration
$\hat{h}$	Mean wing thickness/wing length
I	Moment of inertia
I_b	Moment of inertia for insect body
J	Advance ratio
$\hat{l}$	Distance from anterior tip of body to center of mass/body length
$\hat{l}_1$	Distance from forewing base axis to center of mass/body length
$\hat{l}_2$	Radius of gyration for body/body length
l_b	Body length

$\hat{l}_b$	Body length/wing length
L	Lift
L_b	Lift on the body
m	Body mass
m_k	The k^{th} moment of wing mass about the wing base
$\hat{m}_t$	Thoracic mass/body mass
m_w	Mass of wing pair
$\hat{m}_w$	Wing mass/body mass
M	Pitching moment required to tilt the body to the angle observed in flight
M_p	Passive aerodynamic pitching moment
M_{qs}	Pitching moment predicted by a quasi-steady analysis
n	Wingbeat frequency
o	Distance from point of intersection of wing base axis with sagittal plane to the anterior tip of body
p_w	Wing loading
P	Mechanical power output
P_{acc}	Power required to accelerate wing mass and virtual mass during first half of a half-stroke
P_{ind}	Induced power
P_L	Endpoint of wing chord on leading edge
P_{par}	Parasite power
P_{pro}	Profile power
P_t	Endpoint of wing chord on trailing edge
P^*	Mass-specific mechanical power output
r	Radial position along wing
$\hat{r}$	r/wing length
$\hat{r}_k(m)$	Non-dimensional radius of the k^{th} moment of wing mass
$\hat{r}_k(S)$	Non-dimensional radius of the k^{th} moment of wing area
$\hat{r}_k(v)$	Non-dimensional radius of the k^{th} moment of virtual wing mass
R	Wing length
R'	Maximum projected wing length
Re	Reynolds number
s	Slope of line connecting wingtips
S	Wing area
$S_{frontal}$	Frontal area of insect body
S_k	The k^{th} moment of wing area
S_{plan}	Plan area of insect body
t	Time
$\hat{t}$	Non-dimensional time
U	Air speed
v	Virtual mass of wing pair
$\hat{v}$	Non-dimensional virtual mass of a wing pair
v_k	The k^{th} moment of virtual mass
$v(r,t)$	Flapping velocity

V	Flight velocity
V_i	Induced velocity
$V_{i,norm}$	Normal component of induced velocity
$V_R(r,t)$	Relative velocity
W	Horizontal coverage of film image
Y	Distance from object plane to lens center
α	Angle of attack
α_h	Chord angle relative to horizontal x' axis
$\alpha_{z'}$	Angle between wing chord and z' axis
β	Stroke plane angle
γ	Tilt of resultant vector from vertical
ϵ	Arctan of the ratio of the components of the induced velocity and forward airspeed
η	Roll angle of insect
η_a	Aerodynamic efficiency
θ	Angle of elevation of the wing with respect to stroke plane
$\lvert\Delta\bar{\theta}\rvert$	Difference between mean elevational angles of downstroke and upstroke
$\lvert\Delta\theta_{max}\rvert$	Maximum difference between mean elevational angle of downstroke and upstroke for a given positional angle
κ	Camera tilt above horizontal
ν	Kinematic viscosity of air
ρ	Mass density of air
ρ_b	Mass density of insect body
ρ_w	Mass density of insect wing
ϕ	Positional angle of wing in stroke plane
ϕ_{max}	Maximum positional angle
ϕ_{min}	Minimum positional angle
$\bar{\phi}$	Mean positional angle
Φ	Stroke amplitude
χ	Angle between longitudinal body axis and horizontal
χ_{eff}	Effective body angle
χ_0	Free body angle
χ'	Body angle resulting from passive pitching moments
Ψ	Angle between relative velocity vector and horizontal
ω	Angular velocity of wing during pronation and supination
$\hat{\omega}$	Mean angular velocity/wingbeat frequency

We are indebted to the late Dr Ken Machin for his irreplaceable advice and discussion during the course of this study. Mr Neal Maskell and Mr Dennis Unwin provided invaluable technical expertise. We thank Dr James Mayberry for helpful discussions. The financial assistance of the Marshall Commission, the Smithsonian Tropical Research Institute and the Science and Engineering Research Council is gratefully acknowledged.

References

ALDRIDGE, H. D. J. N. (1986). Kinematics and aerodynamics of the greater horseshoe bat, *Rhinolophus ferrumequinum*, in horizontal flight at various flight speeds. *J. exp. Biol.* **126**, 479–497.

ALFORD, D. V. (1975). *Bumblebees*. London: Davis Poynter.

BAKER, P. S., GEWECKE, M. & COOTER, R. J. (1981). The natural flight of the migratory locust, *Locusta migratoria* L. III. Wing-beat frequency, flight speed, and attitude. *J. comp. Physiol.* **141**, 233–237.

BROWN, R. H. J. (1953). The flight of birds. II. Wing function in relation to flight speed. *J. exp. Biol.* **30**, 90–103.

BUTLER, P. J. & WOAKES, A. J. (1980). Heart rate, respiratory frequency, and wing beat frequency of free flying barnacle geese, *Branta leucopsis*. *J. exp. Biol.* **85**, 213–226.

CARPENTER, R. E. (1985). Flight physiology of flying foxes, *Pteropus poliocephalus*. *J. exp. Biol.* **114**, 619–647.

DAVID, C. T. (1979). Optomotor control of speed and height by free-flying *Drosophila*. *J. exp. Biol.* **82**, 389–392.

DUDLEY, R. & ELLINGTON, C. P. (1990). Mechanics of forward flight in bumblebees. II. Quasi-steady lift and power requirements. *J. exp. Biol.* **148**, 53–88.

ELLINGTON, C. P. (1980). Vortices and hovering flight. In *Instationäre Effekte an Schwingenden Tierflügeln* (ed. W. Nachtigall), pp. 64–101. Wiesbaden: Franz Steiner.

ELLINGTON, C. P. (1984*a*). The aerodynamics of hovering insect flight. II. Morphological parameters. *Phil. Trans. R. Soc. Ser.* B **305**, 17–40.

ELLINGTON, C. P. (1984*b*). The aerodynamics of hovering insect flight. III. Kinematics. *Phil. Trans. R. Soc. Ser.* B **305**, 41–78.

ESCH, H., NACHTIGALL, W. & KOGGE, S. N. (1975). Correlations between aerodynamic output, electrical activity in the indirect flight muscles and wing positions of bees flying in a servomechanically controlled wind tunnel. *J. comp. Physiol.* **100**, 147–159.

GEWECKE, M. (1967). Die Wirkung von Luftströmung auf die Antennen und das Flugverhalten der blauen Schmeissfliege (*Calliphora erythrocephala*). *Z. vergl. Physiol.* **54**, 121–164.

GEWECKE, M. (1970). Antennae: another wind-sensitive receptor in locusts. *Nature, Lond.* **239**, 1263–1264.

GEWECKE, M. (1974). Role of antennae of the dragonfly *Orthetrum cancellatum* in flight control. *Nature, Lond.* **249**, 584–585.

GEWECKE, M. (1975). The influence of the air-current sense organs on the flight behavior of *Locusta migratoria*. *J. comp. Physiol.* **103**, 79–95.

GÖTZ, K. G. (1968). Flight control in *Drosophila* by visual control of motion. *Kybernetik* **4**, 199–208.

GREENEWALT, C. H. (1960). *Hummingbirds*. New York: Doubleday.

HEINRICH, B. (1979). *Bumblebee Economics*. Cambridge: Harvard University Press.

HOLLICK, F. S. J. (1940). On the flight of the dipterous fly *Muscina stabulans* Fallen. *Phil. Trans. R. Ser.* B **230**, 357–390.

JENSEN, M. (1956). Biology and physics of locust flight. III. The aerodynamics of locust flight. *Phil. Trans. R. Soc. Ser.* B **239**, 511–552.

KUTSCH, W. & STEVENSON, P. (1981). Time-correlated flight of juvenile and mature locust: a comparison between free and tethered animals. *J. Insect Physiol.* **27**, 455–459.

MCGAHAN, J. (1973). Flapping flight of the Andean condor. *J. exp. Biol.* **58**, 239–253.

MAGNAN, A. (1934). *La Locomotion Chez les Animaux*. I. *Le Vol des Insectes*. Paris: Hermann et Cie.

NACHTIGALL, W. (1966). Die Kinematik der Schlagflügelbewegungen von Dipteren. Methodische und analytische Grundlagen zur Biophysik des Insektenflugs. *Z. vergl. Physiol.* **52**, 155–211.

NACHTIGALL, W., WIDMANN, R. & RENNER, M. (1971). Uber den "ortsfesten" Flug von Bienen in einem Saugkanal. *Apidologie* **2**, 271–282.

NORBERG, U. M. (1976). Aerodynamics, kinematics, and energetics of horizontal flapping flight in the long-eared bat *Plecotus auritus*. *J. exp. Biol.* **65**, 179–212.

PENNYCUICK, C. J. (1968). Power requirements for horizontal flight in the pigeon *Columba livia*. *J. exp. Biol.* **49**, 527–555.

RAYNER, J. M. V., JONES, G. & THOMAS, A. (1986). Vortex flow visualizations reveal change in upstroke function with flight speed in bats. *Nature, Lond.* **321**, 162–164.

RÜPPELL, G. (1971). Flugmanöver des Gartenrotschwanzes. *Z. vergl. Physiol.* **71**, 190–200.

SCHNELL, G. D. (1974). Flight speeds and wingbeat frequencies of the magnificent frigatebird. *The Auk* **91**, 564–570.

SCHNITZLER, H.-U. (1971). Fledermäuse im Windkanal. *Z. vergl. Physiol.* **73**, 209–221.

SOTOVALTA, D. (1947). The flight-tone (wing-stroke frequency) of insects. *Acta entomol. fennica.* **4**, 1–117.

SPEDDING, G. R. (1986). The wake of a jackdaw (*Corvus monedula*) in slow flight. *J. exp. Biol.* **125**, 287–307.

SPEDDING, G. R. (1987). The wake of a kestrel (*Falco tinnunculus*) in flapping flight. *J. exp. Biol.* **127**, 59–78.

TUCKER, V. A. (1966). Oxygen consumption of a flying bird. *Science* **154**, 150–151.

URQUHART, F. A. (1960). *The Monarch Butterfly*. Toronto: University of Toronto Press.

VOGEL, S. (1966). Flight in *Drosophila*. I. Flight performance of tethered flies. *J. exp. Biol.* **44**, 567–578.

VOGEL, S. (1967). Flight in *Drosophila*. II. Variations in stroke parameters and wing contour. *J. exp. Biol.* **46**, 383–392.

WAINWRIGHT, S. A., BIGGS, W. D., CURREY, J. D. & GOSLINE, J. M. (1976). *Mechanical Design in Organisms*. London: Edward Arnold.

WEIS-FOGH, T. (1956). Biology and physics of locust flight. II. Flight performance of the desert locust (*Schistocerca gregaria*). *Phil. Trans. R. Soc. Ser.* B **239**, 459–510.

WEIS-FOGH, T. (1973). Quick estimates of flight fitness in hovering animals, including novel mechanisms for lift production. *J. exp. Biol.* **59**, 169–230.

WEIS-FOGH, T. & JENSEN, M. (1956). Biology and physics of locust flight. I. Basic principles in insects flight. A critical review. *Phil. Trans. R. Soc. Ser.* B **239**, 415–458.

ZARNACK, W. (1972). Flugbiophysik der Wanderheuschrecke (*Locusta migratoria* L.). I. Die Bewegungen der Vorderflügel. *J. comp. Physiol.* **78**, 356–395.